THE JOURNAL OF BIOLOGICAL CHEMISTRY VOL. 292, NO. 4, pp. 1288–1301, January 27, 2017

A New Method to Study Heterodimerization of Membrane Proteins and Its Application to Fibroblast Growth Factor Receptors*

Received for publication, August 29, 2016, and in revised form, December 5, 2016 Published, JBC Papers in Press, December 7, 2016, DOI 10.1074/jbc.M116.755777

Nuala Del Piccolo, Sarvenaz Sarabipour, and Kalina Hristova[1]

From the Department of Materials Science & Engineering, The Johns Hopkins University, Baltimore, Maryland 21218

Edited by Paul E. Fraser

The activity of receptor tyrosine kinases (RTKs) is controlled through their lateral association in the plasma membrane. RTKs are believed to form both homodimers and heterodimers, and the different dimers are believed to play unique roles in cell signaling. However, RTK heterodimers remain poorly characterized, as compared with homodimers, because of limitations in current experimental methods. Here, we develop a FRET-based methodology to assess the thermodynamics of hetero-interactions in the plasma membrane. To demonstrate the utility of the methodology, we use it to study the hetero-interactions between three fibroblast growth factor receptors—FGFR1, FGFR2, and FGFR3—in the absence of ligand. Our results show that all possible FGFR heterodimers form, suggesting that the biological roles of FGFR heterodimers may be as significant as the homodimer roles. We further investigate the effect of two pathogenic point mutations in FGFR3 (A391E and G380R) on heterodimerization. We show that each of these mutations stabilize most of the heterodimers, with the largest effects observed for FGFR3 wild-type/mutant heterodimers. We thus demonstrate that the methodology presented here can yield new knowledge about RTK interactions and can further our understanding of signal transduction across the plasma membrane.

Receptor tyrosine kinases (RTKs)[2] regulate many key biological processes, including cell survival, growth, differentiation, and migration. There are 58 different RTKs, classified into 20 families based on sequence similarity. An archetypal RTK consists of a ligand-binding extracellular domain, a single-pass transmembrane (TM) domain, and an intracellular (IC) kinase domain (1–5). These receptors are activated upon dimerization, which is known to be a reversible process (6, 7). Dimer formation is required (although not sufficient) for function (2, 6, 8–11), because it brings the two kinases into close proximity, enabling cross-phosphorylation on specific tyrosines. Phosphorylated RTKs trigger many intracellular signaling cascades, including the MAPK, PI3K, PKC, and STAT pathways. These pathways, in turn, determine cell fate and function (1–5, 12, 13).

RTKs play a fundamental role in human development. They are also critical players in the induction and progression of many cancers (1–5, 13–15). Thus, significant efforts have been dedicated to the development of RTK-specific therapies with high specificity and low toxicity. One class of anti-cancer drugs on the market specifically aims to inhibit RTK dimerization, because it is an important regulator of function. The best known example of these drugs is Herceptin, an antibody raised against the extracellular domain of HER2, which is often overexpressed in breast cancer (15, 16). Although Herceptin treatment can significantly improve patient outcomes in some cases, the performance of this treatment and other RTK-targeted molecular therapies has not reached expectations (4, 16, 17). This may be partly due to gaps in basic knowledge about RTK interactions in the plasma membrane.

RTKs readily form homodimers, but they also participate in hetero-interactions with other RTKs, often other members of the same family. Heterodimerization between RTKs is believed to be a means of signal amplification and diversification. RTK heterodimers have been shown to enhance receptor activation and downstream signaling, as compared with homodimers (1, 2, 4, 15, 18, 19). For instance, the ErbB2·ErbB3 heterodimer is known as the most biologically active and the most pro-tumorigenic of all ErbB homodimers and heterodimers (4, 15). However, our understanding of RTK heterodimerization is only rudimentary, in part because of a paucity of methods that provide quantitative information about heterodimer formation (18, 20, 21). Indeed, prior work has relied primarily on qualitative methods such as immunoprecipitation. Thus, the extent of heterodimerization between members of an RTK family remains unknown. Often, even the identities of RTK partners that engage in hetero-interactions are unknown, and this can significantly impede the design of high efficacy therapeutics that target RTK dimerization.

Here, we introduce a novel FRET-based technique that overcomes the limitations of previous methods employed to study heterodimers in the plasma membrane. To demonstrate the utility of the method, we apply it to study heterodimerization within the fibroblast growth factor receptor (FGFR) family of RTKs. We use truncated receptors in which the IC domains have been substituted with fluorescent proteins to allow for FRET detection. Measurements are performed in plasma mem-

* This work was supported by National Institutes of Health Grants GM095930 and GM068619. The authors declare that they have no conflicts of interest with the contents of this article. The content is solely the responsibility of the authors and does not necessarily represent the official views of the National Institutes of Health.

[1] To whom correspondence should be addressed. Tel.: 410-516-8939; E-mail: kh@jhu.edu.

[2] The abbreviations used are: RTK, receptor tyrosine kinase; FGFR, fibroblast growth factor receptor; TM, transmembrane; IC, intracellular; QI, quantitative imaging; ANOVA, analysis of variance; MSE, mean square error.

brane vesicles, derived from cells using an osmotic stress buffer (22). As the receptors are expressed in cells prior to vesicle production, they undergo all post-translational modifications. FRET is measured with the quantitative imaging-FRET (QI-FRET) method (23, 24), which yields donor and acceptor concentrations, in addition to FRET efficiencies, in each vesicle.

The FGFRs regulate the development of the skeletal system (3, 12, 13, 25–27). There are four FGFRs: FGFR1, FGFR2, FGFR3, and FGFR4. Here we focus on FGFR1, FGFR2, and FGFR3, three receptors that have been implicated in many growth disorders (1–3, 5, 8, 13, 27–29). Although originally believed to form dimers only in response to ligand (fgf) binding, FGFRs have been shown to interact and form homodimers even in the absence of ligand (8, 30–34). FGFR homodimerization seems to prime the receptors for efficient activation by the ligand, and thus unliganded FGFR dimers appear to be important intermediates in the signal transduction process (8, 34).

The propensities for homodimer formation have been quantified for full-length FGFR1, FGFR2, and FGFR3, in the absence of ligand (8). The truncated FGFRs also form homodimers, with propensities that are similar to or lower than full-length FGFRs (8, 31–33). We seek to determine the heterodimerization propensities of truncated FGFR1, FGFR2, and FGFR3 and compare them to the homodimerization propensities, in the absence of ligand.

We further seek to examine FGFR heterodimer formation in the presence of two different pathogenic point mutations in FGFR3: G380R and A391E. The G380R mutation in the TM domain of FGFR3 is found in 98% of all achondroplasia cases. Achondroplasia is the most common form of human dwarfism and is characterized by short stature and premature endochondral ossification of long bones (12, 20, 25–28, 33, 35). The A391E mutation, also in the TM domain of FGFR3, causes Crouzon syndrome with acanthosis nigricans. This developmental disorder is characterized by premature ossification of skull bones accompanied by a skin disorder (27, 32, 36–39). Although both mutations introduce a charged amino acid into the TM domain of the same receptor, the resulting phenotypes are substantially different. It has been hypothesized that this difference in phenotype might be explained by disparate perturbations to FGFR heterodimers (27, 36). To directly test this hypothesis, we examine the FGFR1·FGFR3, FGFR2·FGFR3, and wild-type/mutant FGFR3 heterodimers in the presence of both mutations using the new quantitative FRET method, and we compare the results to those of the wild-type using statistical methods.

Results

Development of the Heterodimerization Model—RTK lateral association can be described by monomer-dimer equilibrium models (1, 21, 40). Here, we consider dimer formation when two receptors, X and Y, are capable of forming both heterodimers and homodimers (Fig. 1). In this case, the equilibrium between monomers and dimers is described by three reactions (38),

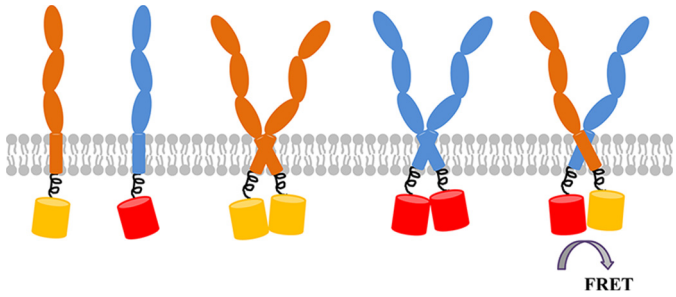

FIGURE 1. **A cartoon representation of the receptor species present in the FRET experiments.** Receptors X and Y are shown in *orange* and *blue*. The IC domains of the receptors are replaced with the fluorescent proteins YFP and mCherry, depicted as *yellow* and *red barrels*, to allow for FRET detection of heterodimer formation. Three possible dimers can form, in accordance with the law of mass action. From *left* to *right*, we show the receptor monomers X and Y, the homodimers XX and YY, and the heterodimer XY. Equations 1 and 2 under "Results" describe the coupled equilibria between the dimers and the monomers. The heterodimer is the only species with both YFP and mCherry and therefore is the only contributor to measured FRET efficiency. All possible species must be accounted for when quantitatively interpreting heterodimer formation from experimental data.

$$[X] + [X] \overset{K_X}{\longleftrightarrow} [XX]$$

$$[Y] + [Y] \overset{K_Y}{\longleftrightarrow} [YY] \qquad \text{(Eq. 1)}$$

$$[X] + [Y] \overset{K_{XY}}{\longleftrightarrow} [XY]$$

where K_X and K_Y are the two macroscopic homodimer association constants, and K_{XY} is the macroscopic heterodimer association constant. The bracket notation indicates two-dimensional species concentration. The three association constants can be written as shown below.

$$K_X = \frac{[XX]}{[X]^2}$$

$$K_Y = \frac{[YY]}{[Y]^2} \qquad \text{(Eq. 2)}$$

$$K_{XY} = \frac{[XY]}{[X][Y]}$$

These relationships are the first key component describing the complex heterodimerization process. The association constants can be used to calculate dimer stability as follows,

$$\Delta G = -RT\,ln\,K \qquad \text{(Eq. 3)}$$

where the standard state is taken as 1 square nanometer per receptor (23). The number of receptors in a cell-derived vesicle is constant over time, and we write the equations of mass conservation as follows,

$$[X_{total}] = [X] + 2[XX] + [XY]$$
$$[Y_{total}] = [Y] + 2[YY] + [XY] \qquad \text{(Eq. 4)}$$

where $[X_{total}]$ and $[Y_{total}]$ are the total concentrations of each receptor species in a given vesicle. If we rearrange the first two statements in Equation 2 to solve for [XX] and [YY] and substitute into Equation 4, we obtain the two statements shown below.

$$[X_{total}] = [X] + 2K_X[X]^2 + [XY]$$
$$[Y_{total}] = [Y] + 2K_Y[Y]^2 + [XY] \quad \text{(Eq. 5)}$$

These statements constitute the second key component describing heterodimerization. Using the quadratic formula (41) to solve Equations 5 for [X] and [Y] and then substituting into the third statement in Equation 2, we arrive at a single equation describing heterodimerization.

$$0 = K_{XY}\left(\frac{2([XY] - [X_{total}])}{1 + \sqrt{1 - 8K_X([XY] - [X_{total}])}}\right) \cdot\left(\frac{2([XY] - [Y_{total}])}{1 + \sqrt{1 - 8K_Y([XY] - [Y_{total}])}}\right) - [XY] \quad \text{(Eq. 6)}$$

This equation is implicit and must be solved numerically. To achieve this, we can employ the MATLAB function "fsolve" in the default setting, which utilizes the trust-region-dogleg algorithm. Solving Equation 6 in this manner produces theoretical predictions for the concentration of heterodimers, which depends on the homodimer association constants, K_X and K_Y, and on the total receptor concentrations, $[X_{total}]$ and $[Y_{total}]$. The total dimer fraction, f_D, is shown below.

$$f_D = \frac{2([XX] + [YY] + [XY])}{[X_{total}] + [Y_{total}]} \quad \text{(Eq. 7)}$$

This value is also equivalent to the sum of the homodimer fractions, $f_{D,XX}$ and $f_{D,YY}$, and the heterodimer fraction, $f_{D,XY}$. The fractions $f_{D,XX}$, $f_{D,YY}$, and $f_{D,XY}$ are defined as shown below.

$$f_{D,XX} = \frac{2[XX]}{[X_{total}] + [Y_{total}]}$$
$$f_{D,YY} = \frac{2[YY]}{[X_{total}] + [Y_{total}]} \quad \text{(Eq. 8)}$$
$$f_{D,XY} = \frac{2[XY]}{[X_{total}] + [Y_{total}]}$$

Next, we turn to solving the heterodimerization problem in the context of FRET experiments. One receptor is labeled with a donor, and the other receptor is labeled with an acceptor. If these two receptors form heterodimers, FRET will occur. The FRET efficiency can be measured with the QI-FRET method as described (23, 24). The measured FRET efficiency can then be corrected for the so-called proximity FRET, to yield the interaction-specific FRET efficiency, E_D. Proximity FRET is a non-negligible FRET efficiency that arises even in the absence of specific interactions, because of the random approach of donors and acceptors within the two-dimensional membrane. We have extensively modeled and measured this phenomenon in previous work, and it mainly depends on the acceptor concentration (42, 43). The corrected FRET efficiency, E_D, is due to heterodimerization only. FRET efficiency is measured through the change in donor fluorescence, so E_D can be written in terms of the concentration of the acceptor-donor complex (that is, the heterodimer) and the concentration of the donor (38, 44, 45),

$$E_D = \frac{[XY]\tilde{E}}{[donor]} \quad \text{(Eq. 9)}$$

where $\tilde{E}$ is the intrinsic FRET, or the FRET efficiency in a given dimer. Intrinsic FRET is the maximum E_D; that is, if all receptors in a vesicle were found in heterodimers, E_D would be equal to $\tilde{E}$. In the general case, $\tilde{E}$ depends on the relative positioning of the two fluorescent proteins (*i.e.* the separation and orientation of the fluorophores) in the dimer. Because the fluorophores are attached to the receptors via long flexible linkers, we can assume that they rotate freely, and thus intrinsic FRET depends mainly on fluorescent protein separation. Under the assumption of free rotation, intrinsic FRET can be written as follows,

$$\tilde{E} = \frac{1}{1 + \left(\frac{d}{R_0}\right)^6} \quad \text{(Eq. 10)}$$

where d is the distance between the donor and acceptor, and R_0 is 53.1 Å, the Förster radius for the YFP-mCherry FRET pair (23, 43). Given an intrinsic FRET value, Equation 10 can be solved for d to estimate fluorophore separation in a given dimer.

Using QI-FRET, we can measure three values per vesicle: donor concentration, acceptor concentration, and FRET efficiency (23, 24). Because one receptor is labeled with the donor, and the other receptor is labeled with the acceptor, the receptor concentrations, $[X_{total}]$ and $[Y_{total}]$, can be directly measured as the donor concentration and acceptor concentration. To calculate heterodimer concentration from experimental data, we rearrange Equation 9 to obtain the following,

$$[XY] = \frac{E_D[donor]}{\tilde{E}} \quad \text{(Eq. 11)}$$

and this relationship is substituted into Equation 6 to yield Equation 12, shown below.

$$0 = K_{XY}\left(\frac{2\left(\frac{E_D[donor]}{\tilde{E}} - [X_{total}]\right)}{1 + \sqrt{1 - 8K_X\left(\frac{E_D[donor]}{\tilde{E}} - [X_{total}]\right)}}\right) \cdot\left(\frac{2\left(\frac{E_D[donor]}{\tilde{E}} - [Y_{total}]\right)}{1 + \sqrt{1 - 8K_Y\left(\frac{E_D[donor]}{\tilde{E}} - [Y_{total}]\right)}}\right) - \frac{E_D[donor]}{\tilde{E}} \quad \text{(Eq. 12)}$$

The quantities $[X_{total}]$, $[Y_{total}]$, E_D, and [donor] are measured experimentally. When K_X and K_Y are known, Equation 12 can be fit to experimental FRET data to find the unknowns K_{XY} and $\tilde{E}$, the two parameters describing heterodimer formation.

Predictions of the Model—Equation 6 predicts the heterodimer concentration [XY], based on each receptor's concentration and the two homodimer association constants. Solving Equation 6 can be a challenging problem. In previous work (19, 38, 46, 47), the ratio of receptor concentrations, $[X_{total}]$:$[Y_{total}]$, was held constant so that all equations can be written as a function of just one receptor concentration, substantially simplifying the mathematical analysis. However, our experiments are performed in a cellular system, which means that the concentration of each receptor, and thus the ratio $[X_{total}]$:$[Y_{total}]$, cannot be controlled. Instead, we must consider and solve Equation 6 as a function of both $[X_{total}]$ and $[Y_{total}]$. In this general case, the theoretical solution is a surface instead of a line. Additionally, because heterodimerization is described by a coupled system of equations, the formation of any dimer species—[XX], [YY], or [XY]—is dependent on the formation propensity of the other two.

Fig. 2 illustrates both of these characteristics using a series of graphs generated over a wide range of possible individual receptor concentrations. In these predictions, the homodimer association constants K_X and K_Y are varied by an order of magnitude, while keeping K_{XY} fixed in all cases. In the *left-hand panels*, the theoretical total dimer fraction, f_D, is represented by a *cyan surface* with contour lines. The total dimer fraction plots can be asymmetrical depending on the relative values of the homodimer association constants. The *right-hand panels* depict the contribution of each dimer species to the total dimer fraction, where the fractional contribution of [XX], [YY], and [XY] are displayed as *violet*, *pink*, and *white surfaces*, respectively. The features of these theoretical solutions are in accordance with the law of mass action. Homodimer fraction is low when the concentration of a given receptor is low and increases with its concentration, and the heterodimer fraction approaches 0 as either $[X_{total}]$ or $[Y_{total}]$ (or both) go to 0. Note that the heterodimer fraction decreases from *panel A* to *panel D*, despite the fact that K_{XY} is the same in all cases. This decrease is due to the relative increases in K_X and K_Y, *i.e.* due to the depletion of monomers as homodimerization increases. These predictions illustrate the complex manner in which receptor concentrations and association constants determine the concentration of each dimer.

FGFR1, FGFR2, FGFR3, FGFR3_G380R, and FGFR3_A391E Form All Possible Heterodimers—We use the model described above to study the heterodimerization of truncated FGFRs, consisting of the extracellular and TM domains of a receptor followed by flexible linkers and fluorescent proteins. First, we consider the hetero-interactions between wild-type FGFR1, FGFR2, and FGFR3. Then we examine these hetero-interactions when FGFR3 carries the point mutations for achondroplasia (FGFR3_G380R) or Crouzon syndrome with acanthosis nigricans (FGFR3_A391E). We investigate three possible wild-type FGFR heterodimers: FGFR1·FGFR2, FGFR1·FGFR3, and FGFR2·FGFR3, and six possible mutant heterodimers: FGFR1·FGFR3_G380R, FGFR2·FGFR3_G380R, FGFR3·FGFR3_G380R, FGFR1·FGFR3_A391E, FGFR2·FGFR3_A391E, and FGFR3·FGFR3_A391E.

For each heterodimer studied, CHO cells are co-transfected with plasmids encoding the two receptor constructs, each labeled with either the donor or the acceptor (and then the labeling scheme is reversed). Twenty-four hours post-transfection, the cells are exposed to an osmotic stress buffer (22) that produces plasma membrane-derived vesicles. These vesicles are collected and then imaged using the QI-FRET method (23, 24). In brief, a confocal microscope is used to image the cross-section of each vesicle in the donor, FRET, and acceptor channels (see Fig. 3 for a representative vesicle). The microscope is calibrated using solutions of free fluorescent protein, so that fluorescence intensity and protein concentration can be directly related, enabling quantitative analysis of images (48). Ultimately, three quantities are measured in each vesicle: donor concentration, acceptor concentration, and FRET efficiency.

Fig. 4 displays the raw data for the nine FGFR heterodimers examined here. The *left-hand panels* show the FRET efficiency as a function of acceptor concentration. The *dark blue right-pointing triangles*, *purple up-pointing triangles*, *green left-pointing triangles*, *light blue diamonds*, and *black squares* represent the FGFR1, FGFR2, FGFR3, FGFR3_G380R, and FGFR3_A391E homodimer FRET data, respectively (previously published (8, 31–33)). In each case, the heterodimer data are represented by *red circles*. Each point corresponds to a single vesicle. The *solid black line* represents the proximity FRET or the FRET efficiency expected because of the nonspecific close approach of labeled receptors (42, 43). For all wild-type and mutant FGFR heterodimers, measured FRET efficiencies exceed proximity FRET, indicating that specific heterodimeric interactions occur in all cases.

Although FRET is plotted in Fig. 4 as a function of acceptor concentration, it also depends on the donor concentration, and thus both concentrations are taken into account in the analysis. The *right-hand panels* in Fig. 4 show the donor concentration *versus* the acceptor concentration for all vesicles analyzed in the heterodimer FRET experiments, again using *red circles*. The substantial variation of the ratio between acceptors and donors occurs because, in a transient transfection experiment, every cell will produce a different amount of each receptor. This variation explains the seemingly wide spread of FRET efficiencies seen in the FRET efficiency *versus* acceptor concentration plots. As discussed previously, a wide range of donor to acceptor ratios, as well as a wide range of concentrations, is an advantage in the QI-FRET methodology, because it ensures a robust fit of a dimerization model to FRET data (24).

FGFR Heterodimer Stabilities and Intrinsic FRET Values Can Be Quantified—We fit the heterodimerization model (Equation 12) to the experimental FRET measurements for each heterodimer pair. We have previously reported all relevant homodimer association constants (8, 31–33). We list those values in Table 1, and we use them as K_X and K_Y in Equation 12. This analysis yields the optimal K_{XY} and $\tilde{E}$. The apparent association constant, K_{XY}, reveals the propensity for heterodimer formation and is used to calculate dimer stability, ΔG_{XY} (Equation 3). Intrinsic FRET, or $\tilde{E}$, is a structural parameter that depends on the positioning of the fluorescent proteins in the dimer but not on the propensity for dimer formation. Note that both K_{XY} and $\tilde{E}$ determine the magnitude of the measured FRET efficiencies, and thus both parameters need to be deter-

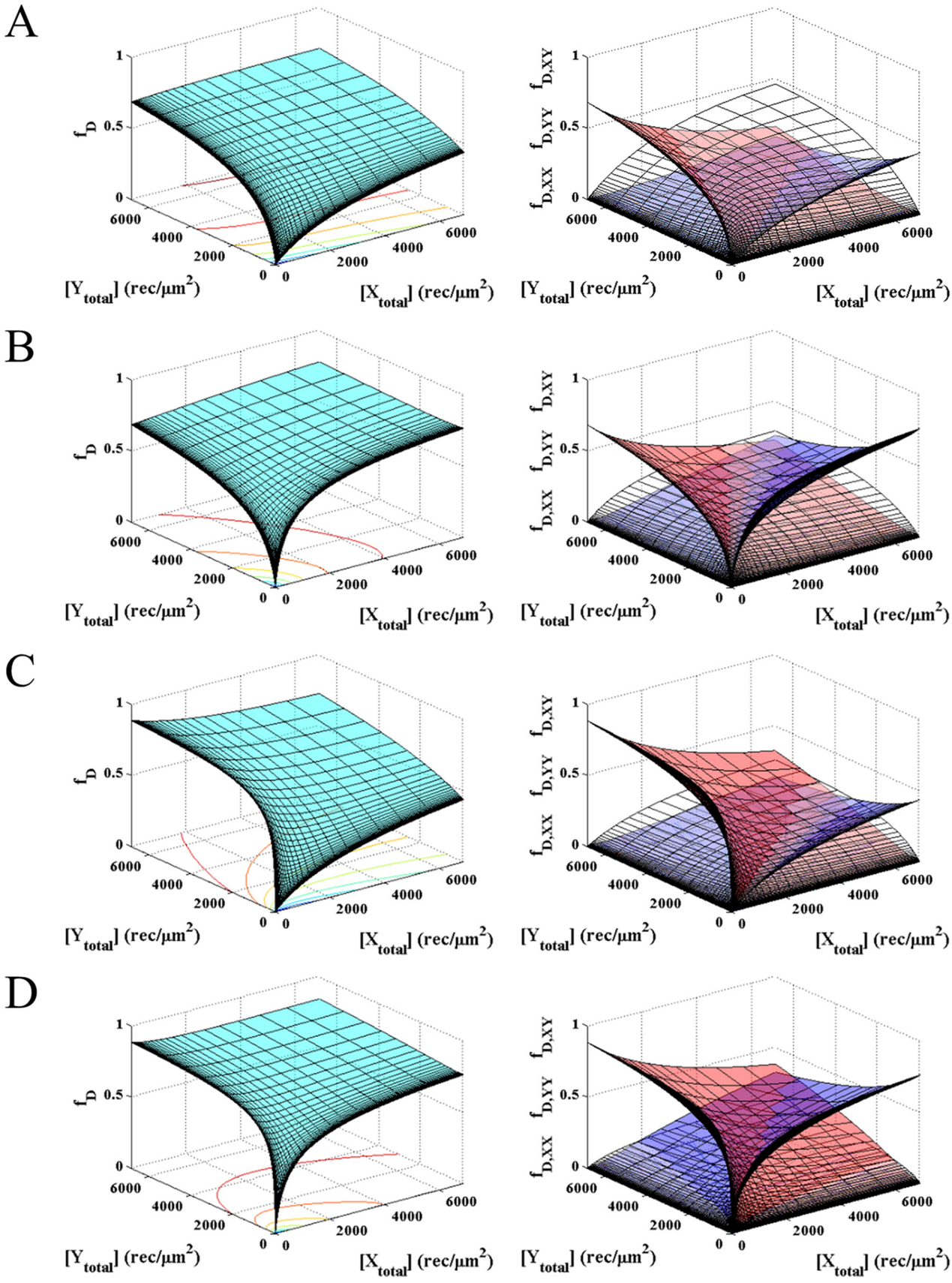
A
B
C
D
f_D
$f_{D,XY}$
$f_{D,YY}$
$f_{D,XX}$
0
0.5
1
6000
4000
2000
0
$[Y_{total}]$ (rec/μm^2)
$[X_{total}]$ (rec/μm^2)

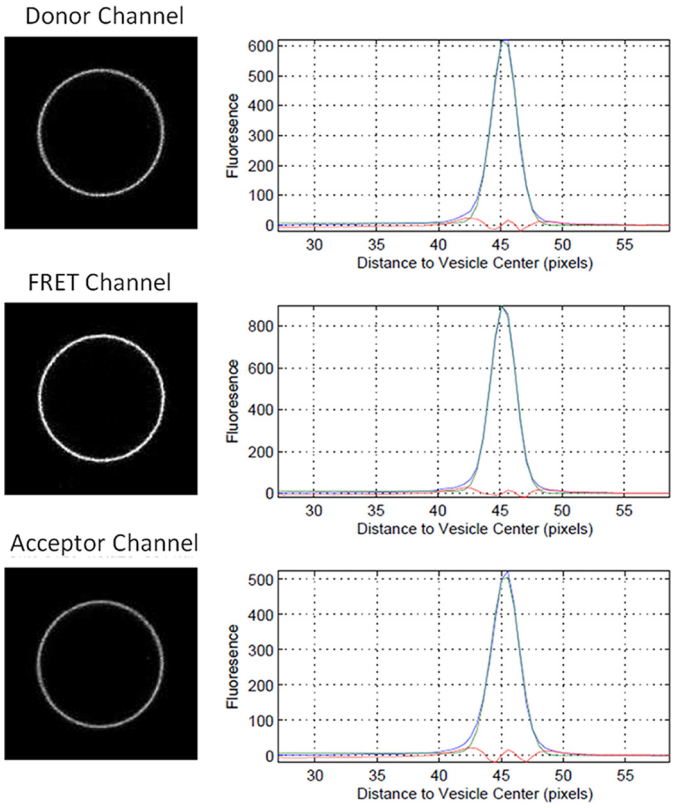

FIGURE 3. **Representative confocal images of a vesicle (*left panels*) and their analysis (*right panels*).** For each vesicle, an image of its cross-section is captured in three channels: donor, FRET, and acceptor. All three images are processed using a MATLAB script previously developed in the lab (23, 24). The program integrates fluorescence intensity along the perimeter of the vesicle membrane cross-section and fits this integrated intensity (*blue line*) with a Gaussian distribution (*green line*), while taking into account the background (*red line*). This process is performed for every vesicle. The QI-FRET method uses these intensities to calculate the donor concentration, the acceptor concentration, and the FRET efficiency in the vesicle (23). In this work, between 250 and 550 vesicles are analyzed for each possible fluorophore labeling scheme of two receptors.

mined and accounted for, to correctly interpret results. In Table 1, we report the optimal K_{XY} and $\tilde{E}$ parameters, along with the calculated dimer stabilities and estimated distances between fluorescent proteins, for all nine heterodimers. In Figs. 5 and 6, we compare experimentally determined values to the optimized heterodimer model for each heterodimer pair. In Fig. 5, the heterodimer concentration [XY] is plotted as a function of both receptor concentrations, with model values (Equation 6) and experimentally determined measurements (Equation 11) shown as a *yellow surface* with contour lines and *open blue* (*above surface*) and *red* (*below surface*) *circles*, respectively. In Fig. 6, the total dimer fraction, calculated using Equation 7, is plotted as a function of the concentration of the two receptors. Model values are displayed as a *cyan surface* with contour lines, and experimentally determined measurements are plotted using *purple circles*.

The wild-type FGFR1·FGFR2, FGFR1·FGFR3, and FGFR2·FGFR3 heterodimer stabilities are -4.5 ± 0.1, -4.8 ± 0.1, and -4.1 ± 0.2 kcal/mol, respectively (Table 1 and Fig. 7*A*). ANOVA tests are performed to compare the ΔG values of homodimers and heterodimers. The stabilities of the FGFR2 and FGFR3 homodimers are statistically the same as each other but different from those of FGFR1 and all the heterodimers. Additionally, the stabilities of FGFR1·FGFR2 and FGFR1·FGFR3 are statistically the same as each other but different from the stability of FGFR2·FGFR3. The ΔG for FGFR1·FGFR3 is also different from that of FGFR1.

We also use ANOVA to compare wild-type intrinsic FRET values. We find that intrinsic FRET is statistically the same for all three wild-type homodimers and the FGFR1·FGFR2 and FGFR2·FGFR3 heterodimers. The intrinsic FRET of the FGFR1·FGFR3 heterodimer is smaller than that of the other five dimers, and this difference is significant. In our experiments, the fluorescent proteins are attached to the TM domain of each FGFR via flexible linkers, so intrinsic FRET predominantly depends on the distance between the fluorescent proteins in the dimers, *d*. Using Equation 10, we calculate this distance under the assumption of free fluorescent protein rotation (an assumption that may not be correct). The relative positioning of the fluorescent proteins, and thus the general dimer architecture, is similar for five of the dimers. In contrast, the inter-fluorophore distance is larger in the FGFR1·FGFR3 heterodimer, suggesting an increase in the separation of the TM domain C termini relative to the other dimers.

We further examine six mutant FGFR heterodimers (Table 1 and Fig. 7, *B–D*). The achondroplasia heterodimers FGFR1·FGFR3_G380R, FGFR2·FGFR3_G380R, and FGFR3·FGFR3_G380R have stabilities of -5.2 ± 0.1, -4.7 ± 0.3, and -5.2 ± 0.1 kcal/mol, respectively. The Crouzon syndrome heterodimers FGFR1·FGFR3_A391E, FGFR2·FGFR3_ A391E, and FGFR3·FGFR3_ A391E have stabilities of -5.3 ± 0.2, -4.5 ± 0.2, and -5.1 ± 0.1 kcal/mol, respectively.

To compare the wild-type and mutant heterodimers, *t* tests are performed on the dimer stability and intrinsic FRET values. The difference between wild-type and mutant dimer stabilities, $\Delta\Delta G_{XY}$, is calculated to assess the effects of mutations on the thermodynamics of dimer formation. Analogously, the difference in intrinsic FRET values, $\Delta\tilde{E}$, is computed to estimate any alteration in dimer architecture. First, we consider the FGFR1·FGFR3 heterodimer. The achondroplasia and Crouzon syndrome mutations both stabilize this heterodimer, by -0.4 ± 0.1 and -0.5 ± 0.1 kcal/mol, respectively.

FIGURE 2. **Theoretical predictions of the heterodimerization model, as a function of the concentration of the two receptors.** This model is based on a coupled system of equations describing the formation of the homodimers XX and YY and the heterodimer XY (see Equations 1 and 2), as well as the mass conservation of the receptors (Equation 4 and 5). The solution of this system is the heterodimerization model (Equation 6), and predictions from this equation are graphed here. The dimer fraction depends on the concentration of each receptor species ($[X_{total}]$ and $[Y_{total}]$), and all three association constants (K_X, K_Y, and K_{XY}). K_X and K_Y are increased from *top* to *bottom*. The *left-hand panels* display total dimer fraction (Equation 7) as a *cyan surface* with contour lines, and the *right-hand panels* display the fractional contribution of each dimer species [XX], [YY], and [XY] (Equation 8) as *violet*, *pink*, and *white surfaces*, respectively. In these plots, we assume a heterodimer association constant of 850×10^{-6} μm^2/rec ($\Delta G_{XY} = -4.0$ kcal/mol). The homodimer association constants are varied by an order of magnitude from $K_{X,1} = 100 \times 10^{-6}$ μm^2/rec and $K_{Y,1} = 500 \times 10^{-6}$ μm^2/rec (*A*) to $K_{X,2} = 10 \times K_{X,1}$ and $K_{Y,2} = K_{Y,1}$ (*B*) to $K_{X,3} = K_{X,1}$ and $K_{Y,3} = 10 \times K_{Y,1}$ (*C*) to $K_{X,4} = 10 \times K_{X,1}$ and $K_{Y,4} = 10 \times K_{Y,1}$ (*D*).

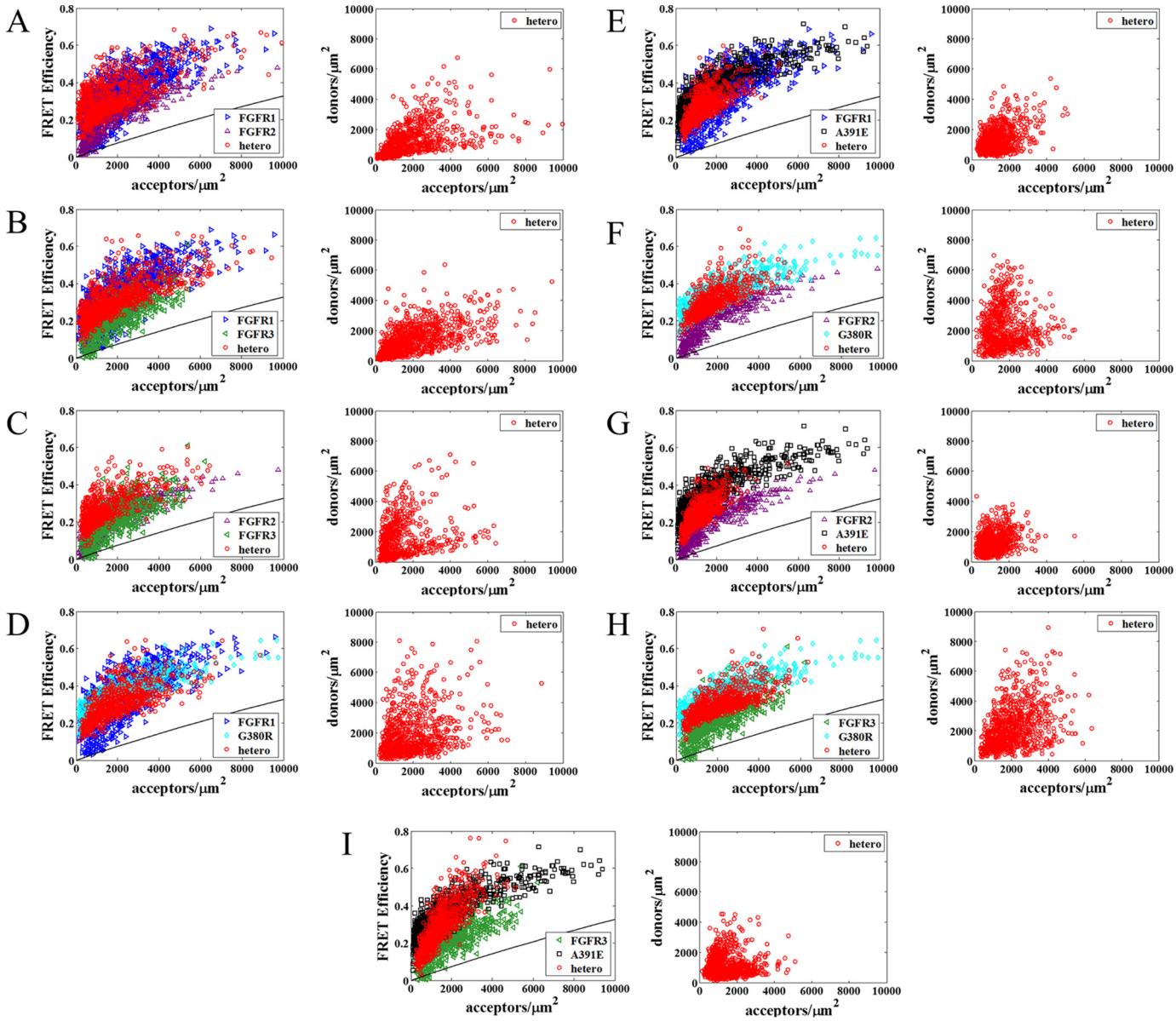

FIGURE 4. **Vesicle FRET data for the wild-type (*A–C*) and mutant (*D–I*) FGFR heterodimers.** The *dark blue right-pointing triangles*, *purple up-pointing triangles*, *green left-pointing triangles*, *light blue diamonds*, and *black squares* represent the FGFR1, FGFR2, FGFR3, FGFR3_G380R, and FGFR3_A391E homodimer FRET data (8, 31–33). The data collected during heterodimer FRET experiments are always shown with *red circles*. For both homodimer and heterodimer data, each point represents a single vesicle. In the *left-hand panels* of *A–I*, the measured FRET efficiencies are plotted as a function of acceptor concentration. Proximity FRET, or the FRET caused by nonspecific close approach of donors and acceptors, is shown as a *black line* (42, 43). The measured FRET efficiencies exceed proximity FRET in every case, which suggests that specific heterodimeric interactions occur for all heterodimers investigated. In subsequent analysis, the measured FRET efficiency is corrected for proximity FRET to find the dimer-specific FRET efficiency. In the *right-hand panels* of *A–I*, donor concentrations are plotted against acceptor concentrations.

Additionally, the achondroplasia mutation increases the intrinsic FRET value.

Next, we turn to the FGFR2·FGFR3 heterodimer. We find that the achondroplasia mutation stabilizes the dimer by -0.6 ± 0.1 kcal/mol and has no effect on intrinsic FRET. The differences between the wild-type and Crouzon syndrome FGFR2·FGFR3 heterodimers are not statistically significant.

The wild-type/mutant FGFR3 heterodimer is slightly different from those described thus far, which all form between two different FGFRs. This heterodimer forms between a wild-type FGFR3 and a FGFR3 with a pathogenic point mutation (either G380R or A391E), and comparisons are made to the wild-type FGFR3 homodimer. The achondroplasia mutation stabilizes the dimer by -1.8 ± 0.1 kcal/mol. The Crouzon syndrome mutation also has a stabilizing effect, with a $\Delta\Delta G_{XY}$ of -1.7 ± 0.1 kcal/mol. Both mutations also decrease the intrinsic FRET value, suggesting that the fluorescent proteins are further apart in the wild-type/mutant FGFR3 heterodimers than in the wild-type FGFR3 homodimer.

Discussion

We Introduce a New Methodology to Study RTK Heterodimerization—Membrane proteins are notoriously challenging to study (49), and detailed information about membrane

TABLE 1

Optimal parameters describing FGFR homodimerization and heterodimerization

Previously published homodimer results (8, 31–33) were used to solve Equation 12, which describes heterodimer formation in FRET experiments. The heterodimer results are listed as averages and standard deviations, as calculated using the bootstrap method (see "Materials and Methods" for details). Dimer stability, ΔG, was calculated from the association constant using Equation 3. Under the assumption of freely rotating fluorophores, the distance between fluorescent proteins in a dimer, d, is estimated using Equation 10.

	Dimer stability		Dimer conformation	
	Association constant, K	ΔG	Intrinsic FRET	d
	$\mu m^2/rec$	*kcal/mol*		*Å*
Homodimers				
FGFR1[a]	$(2336 \pm 484) \times 10^{-6}$	-4.6 ± 0.1	0.50 ± 0.03	53.1 ± 0.7
FGFR2[a]	$(309 \pm 57) \times 10^{-6}$	-3.4 ± 0.1	0.57 ± 0.04	50.7 ± 1.0
FGFR3[a,b]	$(309 \pm 65) \times 10^{-6}$	-3.4 ± 0.1	0.52 ± 0.03	52.4 ± 1.0
FGFR3_G380R[c]	$(6430 \pm 1212) \times 10^{-6}$	-5.2 ± 0.1	0.59 ± 0.01	50.0 ± 0.4
FGFR3_A391E[d]	$(5000 \pm 670) \times 10^{-6}$	-4.8 ± 0.1	0.72 ± 0.02	45.5 ± 0.6
Heterodimers				
FGFR1·FGFR2	$(2109 \pm 379) \times 10^{-6}$	-4.5 ± 0.1	0.52 ± 0.04	52.3 ± 1.3
FGFR1·FGFR3	$(3540 \pm 432) \times 10^{-6}$	-4.8 ± 0.1	0.38 ± 0.02	57.4 ± 0.6
FGFR2·FGFR3	$(988 \pm 308) \times 10^{-6}$	-4.1 ± 0.2	0.53 ± 0.05	52.0 ± 1.9
FGFR1·FGFR3_G380R	$(6428 \pm 1302) \times 10^{-6}$	-5.2 ± 0.1	0.51 ± 0.06	52.6 ± 2.0
FGFR2·FGFR3_G380R	$(2829 \pm 1207) \times 10^{-6}$	-4.7 ± 0.3	0.73 ± 0.20	43.5 ± 9.7
FGFR3·FGFR3_G380R	$(6435 \pm 180) \times 10^{-6}$	-5.2 ± 0.1	0.37 ± 0.01	57.9 ± 0.4
FGFR1·FGFR3_A391E	$(8463 \pm 2715) \times 10^{-6}$	-5.3 ± 0.2	0.48 ± 0.08	53.7 ± 2.9
FGFR2·FGFR3_A391E	$(2106 \pm 714) \times 10^{-6}$	-4.5 ± 0.2	0.78 ± 0.18	41.6 ± 8.6
FGFR3·FGFR3_A391E	$(5356 \pm 551) \times 10^{-6}$	-5.1 ± 0.1	0.40 ± 0.02	56.7 ± 0.8

[a] Data from Ref. 8.
[b] Data from Ref. 31.
[c] Data from Ref. 33.
[d] Data from Ref. 32.

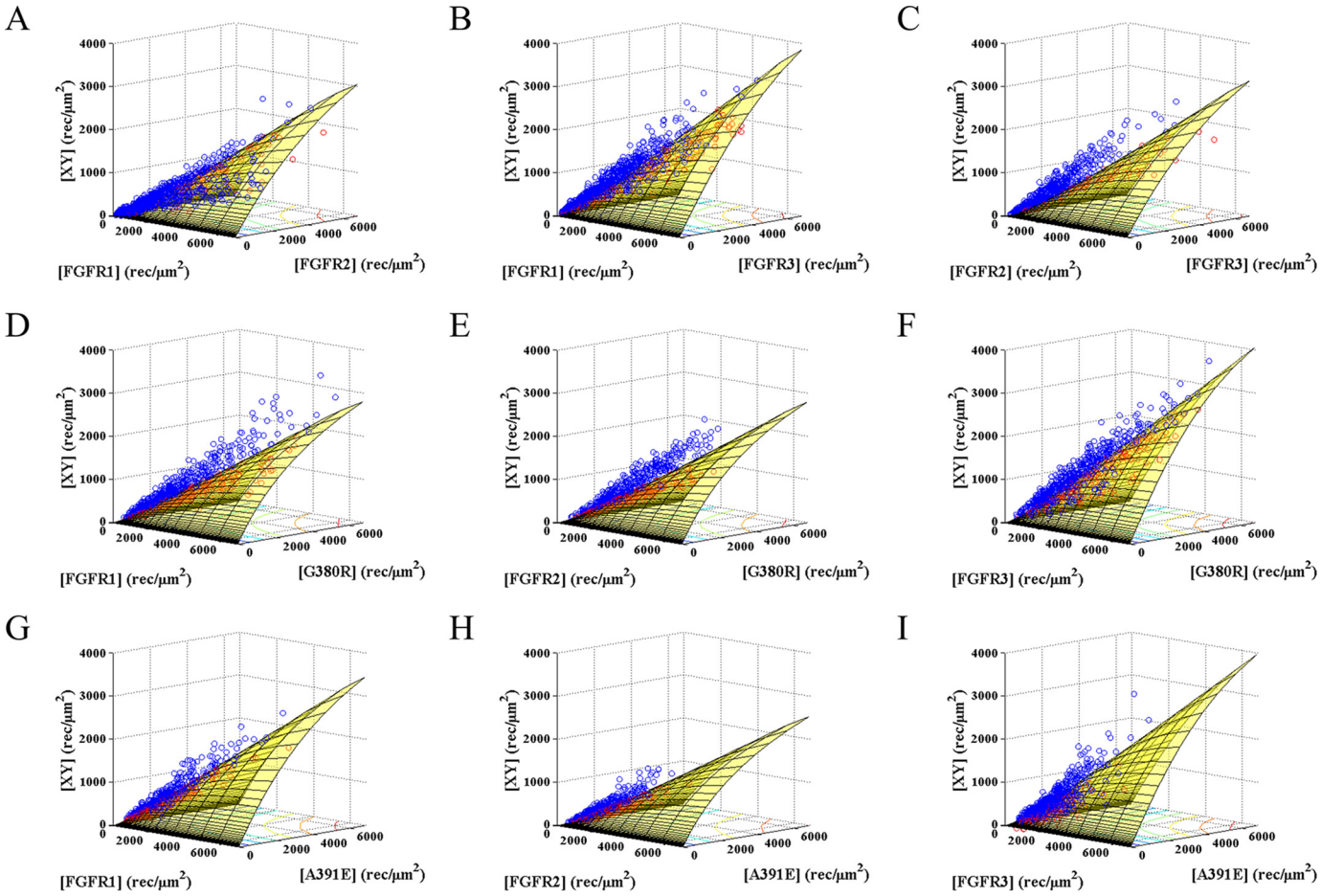

FIGURE 5. **Experimentally determined and theoretically predicted heterodimer concentrations [XY], as a function of the two receptor concentrations.** The model is plotted as a *yellow surface* with contour lines and experimentally determined values are shown as *blue* (*points above model surface*) or *red* (*points below model surface*) *circles*. Experimental heterodimer concentrations are calculated according to Equation 11, and theoretical predictions are made using Equation 6. The best fit values are plotted here for the wild-type (*A–C*), achondroplasia (*D–F*), and Crouzon syndrome (*G–I*) FGFR heterodimer pairs.

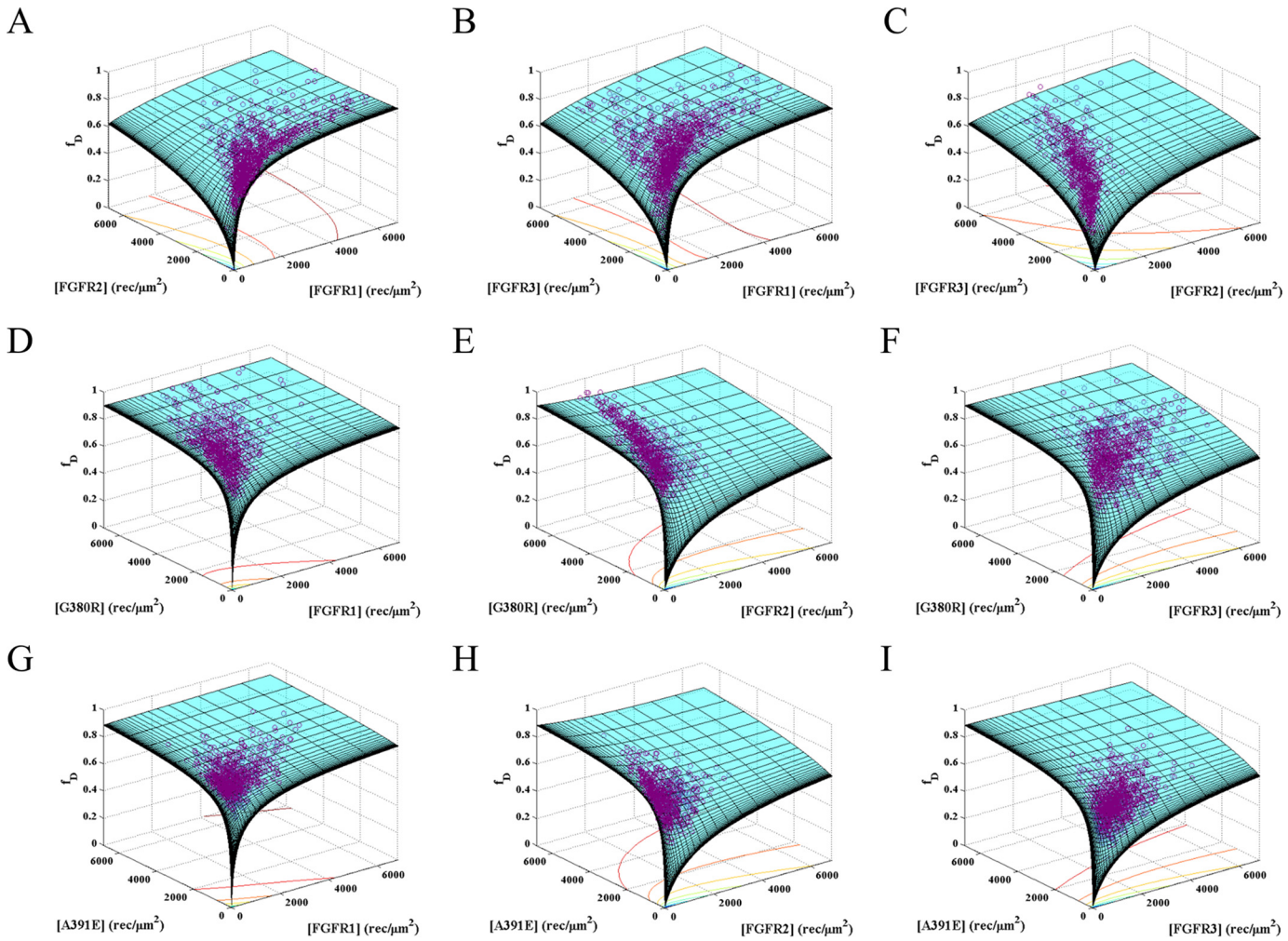

FIGURE 6. **Total dimer fractions.** Equation 7 is used to calculate the total dimeric fraction, f_D, as a function of the receptor concentrations. Experimental data (*purple circles*) are compared with the best fit heterodimerization model (*cyan surface* with *contour lines*). Shown are results for the wild-type (*A–C*), achondroplasia (*D–F*), and Crouzon syndrome (*G–I*) FGFR heterodimer pairs.

protein interactions and structure is elusive, despite active research in the field (50–53). The need for new basic knowledge is underscored by the fact that ~60% of all Food and Drug Administration-approved therapeutics target membrane proteins (54). Biophysical information about drug targets can yield better mechanistic understanding of their function and ultimately can allow for more accurate prediction of drug action and function.

Recently, advances in microscopy have complemented the biochemical assays traditionally used in membrane protein research, producing new insights about membrane protein function (6, 7, 11, 23, 24, 43, 55–57). In this paper, we build on our previous work to develop and implement a quantitative FRET assay for examining RTK heterodimers. The method yields the apparent heterodimer association constant, K_{XY}, and a conformational parameter (intrinsic FRET, or $\tilde{E}$), which has been previously used to assess whether structural changes occur in RTK dimers because of ligand binding or mutations (8, 9, 31–33).

Compared with biochemical methods, FRET offers unique advantages for examining heterodimers. We label one receptor with a FRET donor and the other with a FRET acceptor, so heterodimers have both a donor and acceptor, whereas homodimers have either two donors or two acceptors. Thus, FRET occurs only when heterodimers form. Methods such as SDS-PAGE and Western blotting, on the other hand, struggle to distinguish between RTK homodimers and heterodimers. Challenges arise because receptors are similar in size, so the two complexes cannot be distinguished on a gel. Although immunoprecipitation can report on heterodimer formation, it is limited to qualitative observations and requires the removal of the receptors from the native membrane. Furthermore, in many biochemical methods, the propensity for dimer formation and the structure of that dimer are both known to affect experimental readouts, but their respective contributions usually cannot be separated. The FRET technique described here can report on heterodimer formation in an intact membrane and can uncouple thermodynamic from structural information. However, the receptors are attached to bulky fluorescent proteins, which may perturb interactions in some cases. Furthermore, heterodimerization propensities can only be determined when the homodimerization propensities have already been measured. Finally, no FRET will be detected if the distance

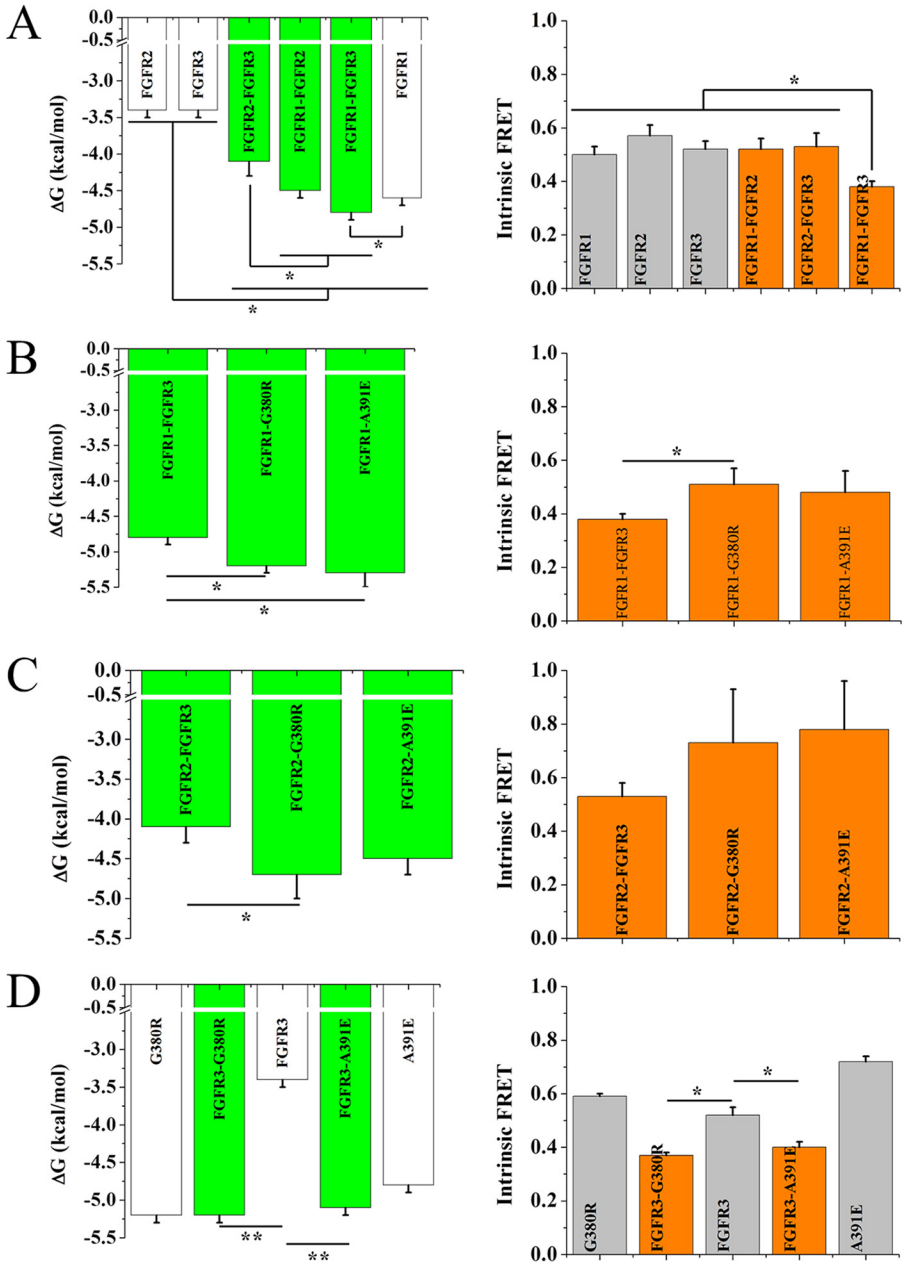

FIGURE 7. **Optimal parameters from the fit.** Results are shown for the wild-type FGFR heterodimers and homodimers (*A*), wild-type and mutant FGFR1·FGFR3 heterodimers (*B*), wild-type and mutant FGFR2·FGFR3 heterodimers (*C*), and wild-type and mutant FGFR3 heterodimers and homodimers (*D*). The *left-hand panels* display heterodimer stabilities (*green bars*) alongside homodimer values (8, 31–33) (*white bars*) to facilitate comparison. Heterodimer stabilities are calculated from association constants using Equation 3. The *right-hand panels* show the intrinsic FRET values, with heterodimer results in *orange* and homodimer values in *gray*. ANOVA is employed to compare wild-type homodimers and heterodimers (see text for results). Unpaired *t* tests are performed to determine the significance of the differences between wild-type and mutant heterodimers. *, $p < 0.05$; **, $p < 0.005$.

between the two fluorophores in the dimer complex exceeds 100 Å, even if a stable dimer forms.

Similar FRET techniques have been discussed in the literature (19, 38, 58), but the methodology presented here improves on previous work in multiple ways. Experiments are performed in cell-derived vesicles that capture many features of the native environment (22, 59). These vesicles closely mimic the diverse lipid and protein content of the plasma membrane (59). The receptors are transiently expressed in the cells prior to vesiculation, so they undergo all relevant post-translational modifications, including glycosylation. In contrast, the previous heterodimerization studies were performed in synthetic lipid vesicles and limited to TM domain peptides.

In previous work on heterodimerization in membranes, the ratio between receptors has been held constant to simplify data analysis (19, 38, 46, 47, 58). The approach that we present has no such limitations and is applicable in cases where the ratio between receptors cannot be controlled, as in cellular studies. The new method is quantitative, yielding heterodimer association constants, despite being performed in a complex system that mimics the native environment. Thus, this FRET method can have broad utility in membrane protein research, because it

TABLE 2

Effects of the achondroplasia and Crouzon syndrome mutations on FGFR heterodimerization

Unpaired *t* tests are performed for the null hypothesis that the wild-type and mutant heterodimers are the same, and the resulting *p* values are shown. ns indicates that any measured difference is not significant. The largest stabilization effects are observed in wild-type/mutant FGFR3 dimers, and these $\Delta\Delta G$ values are accompanied by decreases in intrinsic FRET. FGFR1·FGFR3 is slightly stabilized by each mutation and also experiences an increase in intrinsic FRET due to the achondroplasia mutation. The only statistically significant change in FGFR2·FGFR3 caused by the presence of a mutation is a small increase in stability in the presence of the achondroplasia mutation.

	Dimer stability		Dimer conformation	
	$\Delta\Delta G$ (kcal/mol)	*p* value	$\Delta\tilde{E}$	*p* value
FGFR1·FGFR3_G380R	-0.4 ± 0.1	0.024	$\uparrow$ 0.13	0.021
FGFR1·FGFR3_A391E	-0.5 ± 0.1	0.016	ns	0.103
FGFR2·FGFR3_G380R	-0.6 ± 0.1	0.034	ns	0.173
FGFR2·FGFR3_A391E	ns	0.060	ns	0.0797
FGFR3·FGFR3_G380R	-1.8 ± 0.1	0.000107	$\uparrow$ 0.15	0.0146
FGFR3·FGFR3_A391E	-1.7 ± 0.1	0.000202	$\uparrow$ 0.12	0.0365

can be used to study the heterodimerization propensity of any two membrane proteins.

Wild-type FGFR Homodimers and Heterodimers Have Similar Stabilities and Intrinsic FRET Values—Biochemical methods have previously shown that FGFR heterodimers form and are enzymatically active in cells, in the presence of ligand (20, 29, 60, 61), but the thermodynamics of the association process have not been quantified. Furthermore, FGFR heterodimerization in the absence of ligand has never been investigated. Here, we observe unliganded FGFR heterodimers and for the first time measure the thermodynamic stability of these heterodimers in the plasma membrane. In the absence of ligand, the propensity for heterodimer formation is similar to or larger than that of homodimers (see Table 1 and Fig. 7). When combined with information about the receptor concentrations of the cell, such dimer stabilities can empower prediction of homodimer and heterodimer populations. Therefore, this work can further our understanding of FGFR signaling, which is regulated by the formation of different dimers with unique functions (29, 60, 61).

In this set of experiments, we work with receptors that lack the IC domain, which is replaced with a fluorescent protein on a flexible linker. These truncated receptors can be expressed in a broad concentration range, a requirement for a successful fit of the model to the data, thereby facilitating method development (24). Additionally, the truncation of the receptors increases the likelihood that fluorophores attached to FGFRs in a heterodimer will undergo FRET. RTKs are known to have long unstructured C-terminal tails, and in some cases, this means that fluorescent proteins attached to full-length receptors in a dimer are too far apart to undergo FRET (62).

Contacts between IC domains generally promote, and never inhibit, RTK dimer formation (8, 9, 63–66). Indeed, full-length RTKs have been shown to have stronger propensities for lateral interactions than RTK constructs that lack the IC domain (8). In our previous work with FGFR dimer formation, we measured the contribution of the IC domain to FGFR1, FGFR2, and FGFR3 homodimerization as $\sim$0, -2, and -3 kcal/mol, respectively (8). We expect heterodimer behavior to be similar. Accordingly, our finding that the truncated FGFRs engage in heterodimeric interactions suggests that full-length receptors will also form heterodimers. Furthermore, we expect that the stability of full-length FGFR heterodimers is likely similar to or larger than that measured for truncated FGFR heterodimers.

The Achondroplasia and Crouzon Syndrome Mutations Show Their Largest Effects on the Stability of the FGFR3 Dimer—Table 2 summarizes the changes observed in the FGFR heterodimers caused by the achondroplasia and Crouzon syndrome mutations. The thermodynamics of heterodimerization are perturbed in five of six cases. The largest effects are measured on the dimer stability in the wild-type/mutant FGFR3 dimer. Indeed, the achondroplasia and Crouzon syndrome mutations stabilize this heterodimer by -1.8 ± 0.1 and -1.7 ± 0.1 kcal/mol, respectively. These stabilizations are comparable with those measured for the mutant FGFR3 homodimers (32, 33), suggesting that both mutant homodimers and mutant heterodimers may be important signaling entities in the two developmental disorders. The effects on the FGFR1·FGFR3 and FGFR2·FGFR3 heterodimers, on the other hand, are relatively small. The achondroplasia mutation stabilizes these two heterodimers by -0.4 ± 0.1 and -0.6 ± 0.1 kcal/mol, respectively. The Crouzon syndrome mutation stabilizes FGFR1·FGFR3 by -0.5 ± 0.1 kcal/mol and has no effect on FGFR2·FGFR3. These stabilizations rank among the smaller $\Delta\Delta G$ values that we have measured for pathogenic point mutations in FGFRs (31–33), although these changes might still contribute to the development of the skeletal disorders studied here.

For three of the mutant heterodimers, we observe a statistically significant change in intrinsic FRET, most likely caused by a change in the separation of the fluorescent proteins in the heterodimer. Although the details of how RTK dimer architecture relates to function remain obscure, it is clear that TM domain structure plays a fundamental role in determining signaling properties (8, 9, 67, 68). It is possible that the structural effects (observed as changes in intrinsic FRET) captured in these experiments influence cross-phosphorylation in the heterodimer and potentially contribute to the two phenotypes.

It has been suggested that the phenotypical differences observed between achondroplasia and Crouzon syndrome with acanthosis nigricans might be explained if one of the mutations primarily affects homodimerization, whereas the other mostly influences heterodimerization (27, 36). Our results are inconsistent with this idea, instead suggesting that both mutations have their dominant effects on the FGFR3 homodimer.

Materials and Methods

Plasmids—In this work, 10 different plasmids encoding for five receptors—FGFR1, FGFR2, FGFR3, FGFR3_G380R, and FGFR3_A391E—were used. The IC domains of the receptors were substituted with fluorescent proteins (either YFP or

mCherry) to allow for FRET detection. The fluorescent proteins were attached to the receptor by a flexible $(GGS)_5$ linker, so that they can freely rotate (69). All of these plasmid constructs have been used in previous studies (8, 30, 70, 71).

Cell Culture—CHO cells were cultured in DMEM supplemented with 1.8 g/liter glucose, 1.5 g/liter sodium bicarbonate, 10% fetal bovine serum, and 1 mM nonessential amino acids. The cells were maintained at 37 °C with 5% carbon dioxide and passed every other day.

Transfection—CHO cells were seeded into tissue culture-treated 6-well plates at a density of 2×10^4 cells/well. Approximately 24 h later, the cells were co-transfected with two plasmids, each encoding for one FGFR labeled with either YFP or mCherry. For each heterodimer, the data were collected when one receptor was labeled with the donor and the other one was labeled with the acceptor. The labeling scheme was then reversed, and additional data were collected. All the data for the heterodimer were combined and used in the analysis.

Transfection was performed using FuGENE HD according to the manufacturer's instructions. The total amount of plasmid and the ratio between the two plasmids were both varied in different independent experiments, to collect data in as wide a FGFR expression range as possible. As discussed previously, the wide range of receptor concentrations facilitates the data fitting process (24). Nine possible heterodimers, three wild-type pairs and six pairs with pathogenic point mutations, were characterized in these experiments.

Production of Plasma Membrane Vesicles—Vesiculation of CHO cells was initiated ~24 h after transfection. During this 24-h period, the receptors were synthesized by the cellular machinery, glycosylated, and trafficked to the plasma membrane. Then we used an osmotic stress vesiculation buffer to produce plasma membrane vesicles, as reported previously (22). In short, the cells were rinsed twice with 30% PBS and then incubated overnight at 37 °C in a chloride salt buffer (200 mM NaCl, 5 mM KCl, 0.5 mM $MgCl_2$, 0.75 mM $CaCl_2$, 100 mM Bicine, pH 8.5). In the morning, vesicles were transferred to a 4-well, glass-bottomed chamber slide for QI-FRET analysis. These vesicles constitute a model membrane system with lipid and protein composition similar to the cells from which they are derived (59).

FRET Measurements—FRET was measured using a quantitative fluorescence microscopy technique, QI-FRET, which yields the FRET efficiency, the donor concentration, and the acceptor concentration, in each vesicle. The QI-FRET protocol and equations have been described and discussed at length (please refer to Refs. 23, 24, 31, and 48 for details). Briefly, we used a Nikon Eclipse scanning confocal microscope with a 60× objective to capture images of the cross-section of a given vesicle in three channels: donor (YFP), acceptor (mCherry), and FRET. We calibrated the microscope using solutions of fluorescent protein (72) of known concentration, so that the fluorescence intensity could be directly correlated to fluorophore concentration. Fig. 3 is a representative vesicle imaged in all three channels, alongside the quantitative analysis of its fluorescence intensity across the membrane (including background correction). The intensities measured in the three channels are used in the QI-FRET method to determine the FRET efficiency, the donor concentration, and the acceptor concentration in each vesicle, following the step by step protocol given in Ref. 23.

Statistical Analysis—A two-step process was used to fit the heterodimerization model to the experimental FRET data, ultimately identifying the optimal values for the unknowns K_{XY} and $\tilde{E}$. First, $\tilde{E}$ was fixed, and non-linear least squares (73) (specifically, MATLAB "nlinfit") was used to find K_{XY}. This process was repeated at discreet values of $\tilde{E}$ with a step of 0.01. Second, the mean square error (MSE) was calculated (73) for each of the resulting $(\tilde{E}, K_{XY})$ pairs as follows,

$$\mathrm{MSE} = \frac{\sum_{i=1}^{n} (E_{D_{\mathrm{exper,i}}} - E_{D_{\mathrm{theor,i}}})^2}{n} \qquad \text{(Eq. 13)}$$

where E_D is the interaction-specific FRET efficiency. The experimental value, $E_{D_{exper,i}}$, was measured in each vesicle using the QI-FRET method (23, 24). The theoretical value, $E_{D_{theor,i}}$, was calculated by solving Equation 6 for [XY] using the receptor concentrations in a given vesicle, then substituting into Equation 11 and solving for E_D. n is the total number of vesicles in a given data set. A plot of the MSE as a function of $\tilde{E}$ is U-shaped. The minimum MSE was identified (using the MATLAB function "min") and the $(\tilde{E}, K_{XY})$ pair corresponding to this minimum is taken as the optimal set of parameters.

We note that we use this two-step process because the MATLAB function nlinfit could not fit for both parameters simultaneously, because one of the parameters was consistently imaginary. To confirm that this issue arises from the equations and not the data, we generated simulated heterodimer data sets where we fixed K_{XY} and $\tilde{E}$ and then attempted to use nlinfit to retrieve both parameters simultaneously. Despite the fact that this data is error-free and fits the model perfectly, nlinfit continued to produce imaginary parameter values. Employing the iterative approach, on the other hand, allowed us to successfully retrieve both parameters.

Next, we used the bootstrap method (41) to estimate the errors on these parameters. In the bootstrap method, a given set of data were split into multiple synthetic data sets, and the fitting process was performed on each subset. The optimal parameters from the subsets were used to calculate parameter means and standard deviations.

One-way ANOVA tests were performed to compare the association constants and intrinsic FRET values for wild-type homodimers and heterodimers. First, the bootstrap method was used to refit the previously published homodimer data (8, 31), to make the homodimer and heterodimer data sets comparable. Then the optimal parameters from these fits were compared with K and $\tilde{E}$ for the wild-type heterodimers using one-way ANOVA tests (the MATLAB function "anova1"). We tested the null hypothesis that the three homodimers and three heterodimers are all equivalent. In the case of $p < 0.05$, we rejected the null hypothesis and performed a multiple comparison test (the MATLAB function "multcompare") to determine which homodimers and/or heterodimers are significantly different from the others.

Finally, K_{XY} and $\tilde{E}$ were compared using unpaired t tests (the MATLAB function "ttest2"), to determine the effect of the two

pathogenic point mutations. Each mutant heterodimer was compared with the corresponding wild-type heterodimer, and the wild-type/mutant FGFR3 heterodimers were each compared with the wild-type FGFR3 homodimer. We tested the null hypothesis that the two dimers being compared are not significantly different from each other. The resulting p values were recorded, where $p < 0.05$ indicates that the two groups are significantly different, and $p < 0.005$ indicates a very significant difference.

Author Contributions—N. D. P. developed the model, performed FRET experiments, wrote the software, analyzed the data, and wrote the paper. S. S. performed FRET experiments. K. H. developed the model and wrote the manuscript.

Acknowledgment—We thank Andrew Wimley for technical help.

References

1. Schlessinger, J. (2000) Cell signaling by receptor tyrosine kinases. *Cell* **103,** 211–225
2. Lemmon, M. A., and Schlessinger, J. (2010) Cell signaling by receptor tyrosine kinases. *Cell* **141,** 1117–1134
3. Eswarakumar, V. P., Lax, I., and Schlessinger, J. (2005) Cellular signaling by fibroblast growth factor receptors. *Cytokine Growth Factor Rev.* **16,** 139–149
4. Olayioye, M. A., Neve, R. M., Lane, H. A., and Hynes, N. E. (2000) The ErbB signaling network: receptor heterodimerization in development and cancer. *EMBO J.* **19,** 3159–3167
5. Ornitz, D. M., and Itoh, N. (2015) The fibroblast growth factor signaling pathway. *Wiley Interdiscip. Rev. Dev. Biol.* **4,** 215–266
6. Low-Nam, S. T., Lidke, K. A., Cutler, P. J., Roovers, R. C., van Bergen en Henegouwen, P. M., Wilson, B. S., and Lidke, D. S. (2011) ErbB1 dimerization is promoted by domain co-confinement and stabilized by ligand binding. *Nat. Struct. Mol. Biol.* **18,** 1244–1249
7. Chung, I., Akita, R., Vandlen, R., Toomre, D., Schlessinger, J., and Mellman, I. (2010) Spatial control of EGF receptor activation by reversible dimerization on living cells. *Nature* **464,** 783–787
8. Sarabipour, S., and Hristova, K. (2016) Mechanism of FGF receptor dimerization and activation. *Nat. Commun.* **7,** 10262
9. Sarabipour, S., Ballmer-Hofer, K., and Hristova, K. (2016) VEGFR-2 conformational switch in response to ligand binding. *eLife* **5,** e13876
10. Lin, C. C., Melo, F. A., Ghosh, R., Suen, K. M., Stagg, L. J., Kirkpatrick, J., Arold, S. T., Ahmed, Z., and Ladbury, J. E. (2012) Inhibition of basal FGF receptor signaling by dimeric Grb2. *Cell* **149,** 1514–1524
11. Dietz, M. S., Hasse, D., Ferraris, D. M., Göhler, A., Niemann, H. H., and Heilemann, M. (2013) Single-molecule photobleaching reveals increased MET receptor dimerization upon ligand binding in intact cells. *BMC Biophys.* **6,** 6
12. Krejci, P. (2014) The paradox of FGFR3 signaling in skeletal dysplasia: why chondrocytes growth arrest while other cells over proliferate. *Mutat. Res. Rev. Mutat. Res.* **759,** 40–48
13. Su, N., Jin, M., and Chen, L. (2014) Role of FGF/FGFR signaling in skeletal development and homeostasis: learning from mouse models. *Bone Res.* **2,** 14003
14. He, L., and Hristova, K. (2008) Pathogenic activation of receptor tyrosine kinases in mammalian membranes. *J. Mol. Biol.* **384,** 1130–1142
15. Hynes, N. E., and Lane, H. A. (2005) ERBB receptors and cancer: the complexity of targeted inhibitors. *Nat. Rev. Cancer* **5,** 341–354
16. Drevs, J., Medinger, M., Schmidt-Gersbach, C., Weber, R., and Unger, C. (2003) Receptor tyrosine kinases: the main targets for new anticancer therapy. *Curr. Drug Targets* **4,** 113–121
17. Pantaleo, M. A., Nannini, M., Lopci, E., Castellucci, P., Maleddu, A., Lodi, F., Nanni, C., Allegri, V., Astorino, M., Brandi, G., Di Battista, M., Boschi, S., Fanti, S., and Biasco, G. (2008) Molecular imaging and targeted therapies in oncology: new concepts in treatment response assessment: a collection of cases. *Int. J. Oncol.* **33,** 443–452
18. Tzahar, E., Waterman, H., Chen, X., Levkowitz, G., Karunagaran, D., Lavi, S., Ratzkin, B. J., and Yarden, Y. (1996) A hierarchical network of interreceptor interactions determines signal transduction by Neu differentiation factor/neuregulin and epidermal growth factor. *Mol. Cell. Biol.* **16,** 5276–5287
19. Duneau, J. P., Vegh, A. P., and Sturgis, J. N. (2007) A dimerization hierarchy in the transmembrane domains of the HER receptor family. *Biochemistry* **46,** 2010–2019
20. He, L., Shobnam, N., Wimley, W. C., and Hristova, K. (2011) FGFR3 heterodimerization in achondroplasia, the most common form of human dwarfism. *J. Biol. Chem.* **286,** 13272–13281
21. Gerber, D., Sal-Man, N., and Shai, Y. (2004) Two motifs within a transmembrane domain, one for homodimerization and the other for heterodimerization. *J. Biol. Chem.* **279,** 21177–21182
22. Del Piccolo, N., Placone, J., He, L., Agudelo, S. C., and Hristova, K. (2012) Production of plasma membrane vesicles with chloride salts and their utility as a cell membrane mimetic for biophysical characterization of membrane protein interactions. *Anal. Chem.* **84,** 8650–8655
23. Chen, L., Novicky, L., Merzlyakov, M., Hristov, T., and Hristova, K. (2010) Measuring the energetics of membrane protein dimerization in mammalian membranes. *J. Am. Chem. Soc.* **132,** 3628–3635
24. Sarabipour, S., Del Piccolo, N., and Hristova, K. (2015) Characterization of membrane protein interactions in plasma membrane derived vesicles with quantitative imaging Forster resonance energy transfer. *Acc. Chem. Res.* **48,** 2262–2269
25. Foldynova-Trantirkova, S., Wilcox, W. R., and Krejci, P. (2012) Sixteen years and counting: the current understanding of fibroblast growth factor receptor 3 (FGFR3) signaling in skeletal dysplasias. *Hum. Mutat.* **33,** 29–41
26. Vajo, Z., Francomano, C. A., and Wilkin, D. J. (2000) The molecular and genetic basis of fibroblast growth factor receptor 3 disorders: the achondroplasia family of skeletal dysplasias, Muenke craniosynostosis, and Crouzon syndrome with acanthosis nigricans. *Endocr. Rev.* **21,** 23–39
27. Webster, M. K., and Donoghue, D. J. (1997) FGFR activation in skeletal disorders: too much of a good thing. *Trends Genet.* **13,** 178–182
28. Harada, D., Yamanaka, Y., Ueda, K., Tanaka, H., and Seino, Y. (2009) FGFR3-related dwarfism and cell signaling. *J. Bone Miner. Metab.* **27,** 9–15
29. Bellot, F., Crumley, G., Kaplow, J. M., Schlessinger, J., Jaye, M., and Dionne, C. A. (1991) Ligand-induced transphosphorylation between different FGF receptors. *EMBO J.* **10,** 2849–2854
30. Chen, L., Placone, J., Novicky, L., and Hristova, K. (2010) The extracellular domain of fibroblast growth factor receptor 3 inhibits ligand-independent dimerization. *Sci. Signal.* **3,** ra86
31. Del Piccolo, N., Placone, J., and Hristova, K. (2015) Effect of thanatophoric dysplasia type I mutations on FGFR3 dimerization. *Biophys. J.* **108,** 272–278
32. Sarabipour, S., and Hristova, K. (2015) FGFR3 unliganded dimer stabilization by the juxtamembrane domain. *J. Mol. Biol.* **427,** 1705–1714
33. Sarabipour, S., and Hristova, K. (2016) Effect of the achondroplasia mutation on FGFR3 dimerization and FGFR3 structural response to fgf1 and fgf2: a quantitative FRET study in osmotically derived plasma membrane vesicles. *Biochim. Biophys. Acta* **1858,** 1436–1442
34. Ahmad, I., Iwata, T., and Leung, H. Y. (2012) Mechanisms of FGFR-mediated carcinogenesis. *Biochim. Biophys. Acta* **1823,** 850–860
35. Naski, M. C., Wang, Q., Xu, J., and Ornitz, D. M. (1996) Graded activation of fibroblast growth factor receptor 3 by mutations causing achondroplasia and thanatophoric dysplasia. *Nat. Genet.* **13,** 233–237
36. Cunningham, M. L., Seto, M. L., Ratisoontorn, C., Heike, C. L., and Hing, A. V. (2007) Syndromic craniosynostosis: from history to hydrogen bonds. *Orthod. Craniofac. Res.* **10,** 67–81
37. Delezoide, A. L., Benoist-Lasselin, C., Legeai-Mallet, L., Le Merrer, M., Munnich, A., Vekemans, M., and Bonaventure, J. (1998) Spatio-temporal expression of FGFR 1, 2 and 3 genes during human embryo-fetal ossification. *Mech. Dev.* **77,** 19–30

38. Merzlyakov, M., You, M., Li, E., and Hristova, K. (2006) Transmembrane helix heterodimerization in lipid bilayers: probing the energetics behind autosomal dominant growth disorders. *J. Mol. Biol.* **358,** 1–7
39. Chen, F., Sarabipour, S., and Hristova, K. (2013) Multiple consequences of a single amino acid pathogenic RTK mutation: the A391E mutation in FGFR3. *PLoS One* **8,** e56521
40. He, L., and Hristova, K. (2012) Physical-chemical principles underlying RTK activation, and their implications for human disease. *Biochim. Biophys. Acta* **1818,** 995–1005
41. Press, W. H., Teukolsky, S. A., Vetterling, W. T., and Flannery, B. P. (2007) *Numerical Recipes: The Art of Scientific Computing*, 3rd Ed., Cambridge University Press, Cambridge, UK
42. Wolber, P. K., and Hudson, B. S. (1979) An analytic solution to the Forster energy transfer problem in two dimensions. *Biophys. J.* **28,** 197–210
43. King, C., Sarabipour, S., Byrne, P., Leahy, D. J., and Hristova, K. (2014) The FRET signatures of noninteracting proteins in membranes: simulations and experiments. *Biophys. J.* **106,** 1309–1317
44. You, M., Li, E., Wimley, W. C., and Hristova, K. (2005) Forster resonance energy transfer in liposomes: measurements of transmembrane helix dimerization in the native bilayer environment. *Anal. Biochem.* **340,** 154–164
45. Li, E., You, M., and Hristova, K. (2005) Sodium dodecyl sulfate-polyacrylamide gel electrophoresis and forster resonance energy transfer suggest weak interactions between fibroblast growth factor receptor 3 (FGFR3) transmembrane domains in the absence of extracellular domains and ligands. *Biochemistry* **44,** 352–360
46. Shankaran, H., Wiley, H. S., and Resat, H. (2006) Modeling the effects of HER/ErbB1–3 coexpression on receptor dimerization and biological response. *Biophys. J.* **90,** 3993–4009
47. Samna Soumana, O., Garnier, N., and Genest, M. (2008) Insight into the recognition patterns of the ErbB receptor family transmembrane domains: heterodimerization models through molecular dynamics search. *Eur. Biophys. J.* **37,** 851–864
48. Li, E., Placone, J., Merzlyakov, M., and Hristova, K. (2008) Quantitative measurements of protein interactions in a crowded cellular environment. *Anal. Chem.* **80,** 5976–5985
49. von and Heijne, G. (1999) A day in the life of Dr. K. or how I learned to stop worrying and love lysozyme: a tragedy in six acts. *J. Mol. Biol.* **293,** 367–379
50. Li, E., Wimley, W. C., and Hristova, K. (2012) Transmembrane helix dimerization: Beyond the search for sequence motifs. *Biochim. Biophys. Acta* **1818,** 183–193
51. Cymer, F., Veerappan, A., and Schneider, D. (2012) Transmembrane helix-helix interactions are modulated by the sequence context and by lipid bilayer properties. *Biochim. Biophys. Acta* **1818,** 963–973
52. Fink, A., Sal-Man, N., Gerber, D., and Shai, Y. (2012) Transmembrane domains interactions within the membrane milieu: principles, advances and challenges. *Biochim. Biophys. Acta* **1818,** 974–983
53. Hong, H., Joh, N. H., Bowie, J. U., and Tamm, L. K. (2009) Methods for measuring the thermodynamic stability of membrane proteins. *Methods Enzymol.* **455,** 213–236
54. Overington, J. P., Al-Lazikani, B., and Hopkins, A. L. (2006) How many drug targets are there? *Nat. Rev. Drug Discov.* **5,** 993–996
55. King, C., Stoneman, M., Raicu, V., and Hristova, K. (2016) Fully quantified spectral imaging reveals *in vivo* membrane protein interactions. *Integr. Biol.* (*Camb.*). **8,** 216–229
56. Kenworthy, A. K., Petranova, N., and Edidin, M. (2000) High-resolution FRET microscopy of cholera toxin B-subunit and GPI-anchored proteins in cell plasma membranes. *Mol. Biol. Cell* **11,** 1645–1655
57. Lazar, J., Bondar, A., Timr, S., and Firestein, S. J. (2011) Two-photon polarization microscopy reveals protein structure and function. *Nat. Methods* **8,** 684–690
58. Khadria, A. S., and Senes, A. (2013) The transmembrane domains of the bacterial cell division proteins FtsB and FtsL form a stable high-order oligomer. *Biochemistry* **52,** 7542–7550
59. Sarabipour, S., Chan, R. B., Zhou, B., Di Paolo, G., and Hristova, K. (2015) Analytical characterization of plasma membrane-derived vesicles produced via osmotic and chemical vesiculation. *Biochim. Biophys. Acta* **1848,** 1591–1598
60. Chen, Y., Li, X., Eswarakumar, V. P., Seger, R., and Lonai, P. (2000) Fibroblast growth factor (FGF) signaling through PI 3-kinase and Akt/PKB is required for embryoid body differentiation. *Oncogene* **19,** 3750–3756
61. Ueno, H., Gunn, M., Dell, K., Tseng, A., Jr., and Williams, L. (1992) A truncated form of fibroblast growth factor receptor 1 inhibits signal transduction by multiple types of fibroblast growth factor receptor. *J. Biol. Chem.* **267,** 1470–1476
62. Sorkin, A., McClure, M., Huang, F., and Carter, R. (2000) Interaction of EGF receptor and grb2 in living cells visualized by fluorescence resonance energy transfer (FRET) microscopy. *Curr. Biol.* **10,** 1395–1398
63. Jura, N., Endres, N. F., Engel, K., Deindl, S., Das, R., Lamers, M. H., Wemmer, D. E., Zhang, X., and Kuriyan, J. (2009) Mechanism for activation of the EGF receptor catalytic domain by the juxtamembrane segment. *Cell* **137,** 1293–1307
64. Red Brewer, M., Choi, S. H., Alvarado, D., Moravcevic, K., Pozzi, A., Lemmon, M. A., and Carpenter, G. (2009) The juxtamembrane region of the EGF receptor functions as an activation domain. *Mol. Cell* **34,** 641–651
65. Thiel, K. W., and Carpenter, G. (2007) Epidermal growth factor receptor juxtamembrane region regulates allosteric tyrosine kinase activation. *Proc. Natl. Acad. Sci. U.S.A.* **104,** 19238–19243
66. Endres, N. F., Das, R., Smith, A. W., Arkhipov, A., Kovacs, E., Huang, Y., Pelton, J. G., Shan, Y., Shaw, D. E., Wemmer, D. E., Groves, J. T., and Kuriyan, J. (2013) Conformational coupling across the plasma membrane in activation of the EGF receptor. *Cell* **152,** 543–556
67. Bell, C. A., Tynan, J. A., Hart, K. C., Meyer, A. N., Robertson, S. C., and Donoghue, D. J. (2000) Rotational coupling of the transmembrane and kinase domains of the Neu receptor tyrosine kinase. *Mol. Biol. Cell* **11,** 3589–3599
68. Tamagaki, H., Furukawa, Y., Yamaguchi, R., Hojo, H., Aimoto, S., Smith, S. O., and Sato, T. (2014) Coupling of transmembrane helix orientation to membrane release of the juxtamembrane region in FGFR3. *Biochemistry* **53,** 5000–5007
69. Evers, T. H., van Dongen, E. M., Faesen, A. C., Meijer, E. W., and Merkx, M. (2006) Quantitative understanding of the energy transfer between fluorescent proteins connected via flexible peptide linkers. *Biochemistry* **45,** 13183–13192
70. Placone, J., and Hristova, K. (2012) Direct assessment of the effect of the Gly380Arg achondroplasia mutation on FGFR3 dimerization using quantitative imaging FRET. *PLoS One* **7,** e46678
71. Sarabipour, S., and Hristova, K. (2013) FGFR3 transmembrane domain interactions persist in the presence of its extracellular domain. *Biophys. J.* **105,** 165–171
72. Sarabipour, S., King, C., and Hristova, K. (2014) Uninduced high-yield bacterial expression of fluorescent proteins. *Anal. Biochem.* **449,** 155–157
73. Johnson, M. L., and Faunt, L. M. (1992) Parameter estimation by least-squares methods. *Methods Enzymol.* **210,** 1–37